Lappeenranta-Lahti University of Technology LUT
School of Energy Systems
Degree Programme in Electrical Engineering
Master's Thesis
2020

Atte Putkonen

DETECTION OF TORSIONAL RESONANCE FREQUENCY WITH VARIABLE FREQUENCY DRIVE

Examiners: Professor Olli Pyrhönen
D.Sc. Niko Nevaranta
Supervisor: D.Sc. Timo Holopainen

Abstract

Atte Putkonen
Detection of torsional resonance frequency with variable frequency drive
Master's Thesis
Lappeenranta 2020
53 pages, 23 figures and 5 tables

Examiners: Professor Olli Pyrhönen
D.Sc. Niko Nevaranta
Supervisor: D.Sc. Timo Holopainen

Keywords: Torsional vibrations, variable frequency drive, identification, mechanical resonance

Vibrations generated in the drive train can be a serious problem for the reliability and safety of the system. Usually the problems are related to the lowest torsional mode. Typically, the measurements needed for the torsional analysis require external tools and skilled personnel, which tend to be expensive. The rising reliability and safety requirements in the industry lead to increased usage of variable frequency drives (VFD) for improved control of the machine. The usage of the VFD to identify the mechanical characteristics would provide reliability to the non-existing and also to the existing vibration analysis.

In this master's thesis the identifiability of the lowest torsional frequency resonance with VFD is studied by simulations and experimental measurements. The studied signals are stator current, rotational speed and electromagnetic torque. Pseudo random binary sequence (PRBS) is used as the excitation signal for the identification. Welch's modified peridograms are used for spectral analysis of the signals. The reference resonance frequency was identified with the encoder feedback. The closed-loop experiments, where the motor was controlled with speed feedback from either encoder or estimator, show positive results for the rotational speed signal. When using the estimator the errors of the identified resonance frequencies of the tested cases were < 5 %.

Tiivistelmä

Atte Putkonen
Vääntövärähtelyn ominaistaajuuden havainnointi taajuusmuuttajalla
Diplomityö
Lappeenranta 2020
53 sivua, 23 kuvaa and 5 taulukkoa

Työn tarkastajat: Professori Olli Pyrhönen
TkT Niko Nevaranta
Työn ohjaaja: TkT Timo Holopainen

Avainsanat: Vääntövärähtely, taajuusmuuttaja, identifiointi, mekaaninen resonanssi

Voimansiirtolinjalla tapahtuva värähtely voi aiheuttaa vakavia ongelmia järjestelmän luotettavuudelle ja turvallisuudelle. Useimmiten ongelmat liittyvät vääntövärähtelyn alimpaan muotoon. Vääntöanalyysiin tarvittavat mittaukset vaativat yleensä ulkoisia mittalaitteita sekä ammattitaitoista henkilökuntaa, minkä takia tämä on kallista. Teollisuuden kasvavat luotettavuus- ja turvallisuusvaatimukset johtavat sähkökäyttöjen yleistymiseen, mikä mahdollistaa tarkemman säädön koneille. Sähkökäyttöjen hyödyntäminen mekaniikan identifiointiin toisi luotettavuutta värähtelyanalyysiin. Näin ollen kriittisiä nopeuksia pystyttäisiin varmemmin välttämään.

Tässä diplomityössä tutkitaan vääntövärähtelyn alimman resonanssin havaittavuutta taajuusmuuttajalla simulaatioiden ja käytännön mittauksien avulla. Tutkittavat signaalit ovat moottorin staattorivirta, pyörimisnopeus sekä vääntömomentti. Herätesignaalina identifioinnissa käytetään PRBS (pseudo random binary sequence) signaalia. Tutkittavia signaaleja analysoidaan taajuustasossa käyttäen Welchin menetelmää. Vertailuresonanssi identifioitiin takaisinkytketystä systeemistä käyttämällä mitattua nopeutta. Suljetun systeemin mittauksien perusteella, missä nopeuden takaisinkytkentä oli joko anturilta tai estimaattorilta, resonanssi oli selvästi havaittavissa pyörimisnopeudesta. Testatuissa tapauksissa, pyörimisnopeudesta identifioitujen resonanssien virhe oli alle 5 % anturittomassa tapauksessa.

Acknowledgements

This study was carried out in Lappeenranta-Lahti University of Technology, Finland, between 2019 and 2020. The research was made in collaboration with ABB Oy.

I would like to thank ABB for providing the interesting and challenging master's thesis topic. I want to express my gratitude for D.Sc. Niko Nevaranta and D.Sc. Markku Niemelä from LUT University and D.Sc. Timo Holopainen and M.Sc. Olli Liukkonen from ABB for important comments and guidance during this project. Special thanks go to Eino Oilinki and Antti Holopainen for setting up the experimental setup and for the help and humor in the laboratory.

The biggest thanks go to my friends and family for their support through my life. Studying in Lappeenranta have been the most fulfilling time of my life. For the many unforgettable moments I have had during the studies, I would especially like to thank the student organization Sätky ry and the tech students music organization TeMu ry. Thank you.

Atte Putkonen
April 2020
Lappeenranta, Finland

Contents

Abstract

Tiivistelmä

Acknowledgements

Nomenclature **7**

1 Introduction **10**
1.1 Motivation of the study 11
1.2 Research questions and goals 12
1.3 Research methods and the structure of thesis 12

2 Torsional vibrations **13**
2.1 Analyzing methods 14
2.2 Excitation sources 17
2.3 Effects to mechanics 19
2.4 Compensation and detection methods 19

3 System identification **21**
3.1 Excitation signals 23
3.1.1 Pseudo-random binary sequence 24
3.2 Spectral analysis 28

4 Closed-loop experimental results **30**
4.1 Frequency converter ACS880-01 30
4.2 ABB AC500 PLC and the PRBS generation 32
4.3 Measurements and results 34
4.3.1 Torque measurement analysis 36
4.3.2 Speed measurement analysis 37
4.3.3 Current measurement analysis 37
4.4 Discussion 40

5 Direct on line application **43**
5.1 Simulation model and results 43
5.2 Experimental results 46

6 Conclusions and summary **48**

References **50**

Nomenclature

Latin alphabet

$\hat{G}(\mathrm{j}\omega)$	Frequency response estimate
$\hat{S}_{\mathrm{uu}}(\mathrm{j}\omega)$	Welch's power spectral density estimate of input signal
$\hat{S}_{\mathrm{uy}}(\mathrm{j}\omega)$	Cross power spectral density estimate between input and output
$\mathbf{C}_{\mathrm{t}}$	Torsional damping matrix
$\mathbf{J}$	Moment of inertia matrix
$\mathbf{K}_{\mathrm{t}}$	Torsional stiffness matrix
j	Imaginary unit
A	Amplitude
b	Friction coefficient
c_{t}	Torsional damping
d	Shaft diameter
f_{ares}	Anti-resonance frequency
f_{bw}	Frequency bandwidth
f_{exc}	Excitation frequency
f_{gn}	Generating frequency
f_{in}	Input frequency of the frequency converter
f_{out}	Output frequency of the frequency converter
f_{res}	Resonance frequency
f_{r}	Frequency resolution
f_{s}	Sampling frequency
G	Shear modulus
h	Number of registers
i	Index
i_{d}	Direct axis current
I_{p}	Polar second moment of area
i_{q}	Quadrature axis current
I_{s}	Stator current
J	Moment of inertia
K	Number of sections
k	Discrete time instant
k_{M}	Discrete time instant of the section data
K_{P}	Proportional gain

k_{t}	Torsional stiffness
L	Number of samples
l	Length of a shaft
L_{mag}	Magnetizing inductance
$L_{\mathrm{s}\sigma}$	Stator leakage inductance
$L'_{\mathrm{s}\sigma}$	Rotor leakage inductance reduced to stator
M	Number of data points in one section
m	Positive or negative integer
N	Period length
n	Positive integer
n_{N}	Nominal rotational speed
p	Number of pole pairs
P_{N}	Nominal power
r	Excitation signal
R'_{r}	Rotor resistance reduced to stator
R_{s}	Stator resistance
S	Scaling factor
s	Laplace-domain variable
T	Duration of period
t	Continuous time
T_{I}	Integration time
u	Input
w	Spectral window
y	Output
Z	Unit delay

Greek alphabet

$\boldsymbol{\tau}$	Torque vector
$\boldsymbol{\theta}$	Vector of torsional twist angles
ω	Angular frequency
ω_{n}	Natural frequency
τ	Torque
τ_{N}	Nominal torque
θ	Torsional twist angle

Subscripts

l	Load
m	Motor

Abbreviations

CSI	Current Source Inverter
DFT	Discrete Fourier Transform
DOL	Direct On Line
DTC	Direct Torque Control
FBA	Fieldbus Adapter
MLBS	Maximum Length Binary Sequence
PLC	Programmable Logic Controller
PLL	Phase Locked Loop
PRBS	Pseudo-Random Binary Sequence
PSD	Power Spectral Density
VFD	Variable Frequency Drive
VSI	Voltage Source Inverter

1 Introduction

Vibration analysis is an important part in a rotational system design. The undesirable vibrations generate energy losses and dynamical stresses in the system. In practice, since fully rigid bodies don't exist, every system have some amount of vibrations. In most cases the rotating systems of the industry are powered with an electric motor. The rotary motion of the shaft can then be converted to linear movement when necessary. The vibration occurring on the shaft can be axial, lateral and torsional. Generally, axial vibrations occur along the shaft and the effects are uniform on the whole cross-section of the shaft. However, its effects matter mainly in jet engine applications or such where thrust force is generated. Lateral vibrations can be seen as displacement of the shaft in horizontal or vertical directions, which may lead to wearing of the bearings. Whereas axial and lateral vibrations are relatively easy to detect from the non-rotating parts of the system, torsional vibrations can remain unnoticed damaging the shaft until breakage. Torsional vibrations cause the shaft to twist around its axis. Typically torsional vibrations are created by fast variations or transients of the load. Detecting torsional vibrations usually require external measurement instruments. (Friswell et al., 2010) With careful vibration analysis a better performance and a longer life time of the mechanical system can be achieved by

- securing the safe operation of the mechanical structure,
- detecting the critical frequencies that should be avoided or damped,
- reducing the possible noise issues (Vulfson, 2015).

Larger machines are typically designed for a specific system. In that case, the system's parameters, such as inertias and other detailed information, are known and the system's dynamic analysis can be performed beforehand. Analysis can be carried out during the design procedure and the possibly problematic vibrations can be taken into account in the mechanical design as well as in the controller design. However, smaller machines are more general products and thus the required information might not be

available or it is too expensive to determine.

Electrical motors are widely used in industrial applications like pumps, blowers and compressors. By controlling the motor with a variable frequency drive (VFD) the performance of the electrical drive can be improved with accurate speed and torque control in varying loading conditions. Many commercial VFDs have an internal model of the controlled motor. This enables the estimation of important motor variables, such as flux, rotor position and rotation speed. These estimates can be used in the control loop of the drive even without any additional sensors which can simplify the setup, reduce the cost of the system and improve the performance of the drive. Typically, the motor model parameters are identified during commissioning of the system by performing an identification run which usually is an integrated feature of the VFD. Many control methods, such as direct torque control (DTC), are based on the estimated variables (Kaukonen, 1999).

1.1 Motivation of the study

Typically the torsional natural frequency is an estimate obtained from the vibration analysis. The field measurement instruments for the identification of torsional modes and frequencies include torsiographs, strain gauges and rotary encoders. Generally, measurement of the torsional vibration is based on the detecting the relative displacement between two points on the shaft. However, the whole shaft of the system is usually not totally exposed and hence the placement of the measurement devices require careful planning. This leads to a case where the skilled personnel must travel on site to gather the useful data of the system which tends to be time consuming and expensive process.

Any rapid solution to detect the torsional natural frequency on site does not exist or is unknown to the author of this thesis. Benefits of a feature, like the existing identification run in frequency converters, to identify the mechanical resonance would be beneficial:

- Validation of the non-linear torsional stiffness of the coupling for dif-

ferent loading conditions

- Verification of the critical and the safe operating speed ranges
- Usage in a condition monitoring system to determine maintenance intervals
- Troubleshooting for the possible torsional issues

1.2 Research questions and goals

The goal of this thesis is to investigate if the first torsional natural frequency in the power transmission line can be identified using VFD. The research questions are as follows:

- Can the VFD be used to detect lowest frequency component of the vibration without external components?
- What excitation signal will result to robust identification of the lowest torsional mode?

The studied signals are motor's stator current, rotational speed and electromagnetic torque.

1.3 Research methods and the structure of thesis

The research is carried out with literature review of the torsional vibrations in general. Then a theoretical approach to the system identification and the used analyzing methods are presented. The analyzing methods are tested experimentally on the laboratory setup. First, by using a measured feedback signal the natural frequency of the experimental two-mass system is identified and the identifiability from the studied signals is tested experimentally with a closed-loop application. The results are then compared to a sensorless case. Finally, the current signal is studied in a direct on line (DOL) application with simulations and experimental measurements.

2 Torsional vibrations

When analyzing basic rotating systems, the rotor is often treated as a rigid body. If considering a system with two moments of inertia this means that the angular motion on them both is assumed to be equal. Of course, this simplification is useful, for example, when the dynamics of the subsystem to be rotated are analyzed. In that case it is a justified approximation since the stiffness of the shaft is usually much higher than the stiffness of the subassembly, like a belt drive. However, at least with long rotors and coupled shafts the angular velocity on the different ends can vary considerably. These fluctuations in angular velocity cause the rotor to twist about its axis and are called torsional vibrations. Sometimes they are also referred as angular vibration, transmission error or jitter. Torsional vibrations affect torque and speed and hence are also of interest in the electrical drives point of view (Niiranen, 2000). Despite the torsional vibrations are occurring on the angular velocity the torsional resonance frequencies are usually not dependent on the operating speed (Friswell et al., 2010).

Torsional flexibility is formed due to elastic joints between two or more rigid bodies. Fig. 2.1 shows a system of two inertias that are connected together with a flexible coupling, e.g. an electrical motor to a load. The J_1 and J_4 are the moments of inertia of the motor and load, respectively. The k_t and the c_t are the torsional stiffness and torsional damping, respectively, of the corresponding shaft section. The coupling can be modeled with two inertial discs and a shaft with a torsional stiffness of the coupling (Corbo and Malanoski, 1996; Niiranen, 2000). The J_2 and J_3 are the moments of inertia of the two halves of the coupling. The shafts between the discs represent torsional springs. By applying torque on the disc 1 it causes the shaft to twist for an amount that depends on the torque and the spring constant. When the stress on the shaft is released the spring-like effects cause the discs to oscillate. (Corbo and Malanoski, 1996) Torsional stiffness of a single shaft part is defined by material properties and can be calculated for shafts with circular cross-sections, as follows

$$k_\mathrm{t} = \frac{\tau}{\theta} = \frac{GI_\mathrm{p}}{l} = \frac{\pi G d^4}{32l}, \tag{2.1}$$

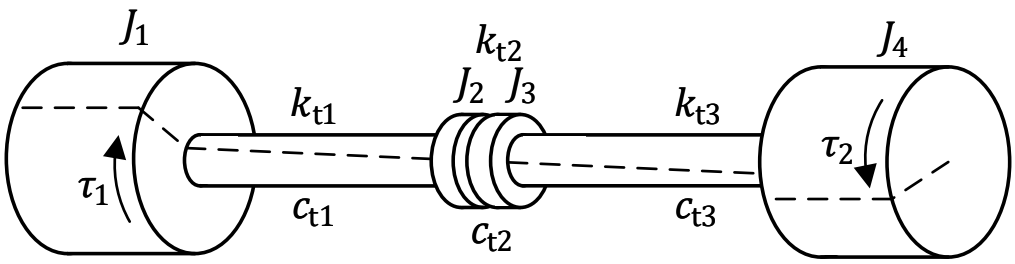

Figure 2.1: A mechanical model of two coupled inertias (e.g. an electrical motor connected to a load with a coupling). The first mode shape of torsional vibration is shown with the dashed line.

where the τ is the applied torque, the θ is the relative twist angle of the shaft section, the G is the shear modulus (modulus of rigidity) which is a material property, the I_p is the polar second moment of area, the d is the shaft diameter and the l is the length of shaft section (Friswell et al., 2010; Holopainen et al., 2013). It's clear that with longer shaft the torsional stiffness decreases which allows the shaft to twist more.

2.1 Analyzing methods

The analysis of the torsional vibrations must be done for the whole shaft train. The shaft train could consist of coupled machines, gears, pinions etc. By changing any component of the shaft train the change in the torsional characteristics can be substantial (Corbo and Malanoski, 1996). The torsional analysis is an important part of the mechanical design since if there might be potentially problematic frequencies present in the operating range of the motor. In that case, the location of the frequencies can be manipulated by changing the couplings for instance. For better understanding, the torsional vibrations are often compared to axial vibrations where the equilibrium can be seen clearly, e.g. a spring-mass system. In fact torsional vibrations' natural frequencies can be analyzed similarly to the spring-mass system. (Friswell et al., 2010) In actual systems there would

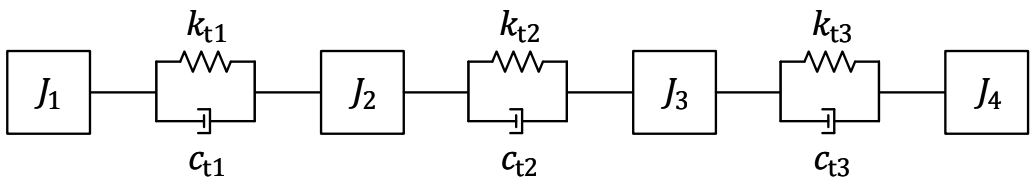

Figure 2.2: A block diagram representation of the mechanical model shown in Fig. 2.1

be some damping elements also, however the preliminary analysis is often carried out on an undamped system to ease the calculations. The error of the calculated natural frequencies with an undamped model is usually negligible (Corbo and Malanoski, 1996).

An example of a mechanical model is presented in Fig. 2.2. The model can be considered as a representation of the system dynamics shown in Fig. 2.1. As stated above the damping can be ignored without significant errors in the calculations. The equation of motion for the rotating system is

$$\mathbf{J}\ddot{\boldsymbol{\theta}} + (\mathbf{C}_{\mathrm{t}}\dot{\boldsymbol{\theta}}) + \mathbf{K}_{\mathrm{t}}\boldsymbol{\theta} = \boldsymbol{\tau}(t), \tag{2.2}$$

where $\mathbf{J}$ is the moment of inertia matrix, $\boldsymbol{\theta} = \begin{bmatrix}\theta_1, & \theta_2, & \theta_3, & \theta_4\end{bmatrix}^{\mathrm{T}}$ is the vector representing the twist angles, $\mathbf{K}_{\mathrm{t}}$ is the matrix representing the torsional stiffnesses, $\mathbf{C}_{\mathrm{t}}$ is the matrix representing the torsional dampings, and the $\boldsymbol{\tau}(t)$ is the vector of the time dependent torque affecting the corresponding inertia. In the case of free vibration the $\boldsymbol{\tau}(t) = 0$ and the (2.2) can then be solved as an eigenvalue problem. The natural frequencies, $\boldsymbol{\omega}_{\mathrm{n}}$, can then be calculated as square root of the eigenvalues whereas the corresponding eigenvectors represent the mode shape of the vibration. (Friswell et al., 2010) The number of the modeled discs equal to the number of the calculable natural frequencies from which one is always located at the zero frequency and represents the rigid body mode. Neglecting the damping coefficients in Fig. 2.2, the matrix notation for the $\mathbf{J}$ and $\mathbf{K}_{\mathrm{t}}$ can be written as (Friswell et al., 2010)

$$\mathbf{J} = \begin{bmatrix} J_1 & 0 & 0 & 0 \\ 0 & J_2 & 0 & 0 \\ 0 & 0 & J_3 & 0 \\ 0 & 0 & 0 & J_4 \end{bmatrix}, \mathbf{K_t} = \begin{bmatrix} k_{t1} & -k_{t1} & 0 & 0 \\ -k_{t1} & k_{t1}+k_{t2} & -k_{t2} & 0 \\ 0 & -k_{t2} & k_{t2}+k_{t3} & -k_{t3} \\ 0 & 0 & -k_{t3} & k_{t3} \end{bmatrix}. \quad (2.3)$$

The eigenvalue method is straightforward for larger systems. However, most of the mechanical systems can be simplified to a two-mass system which is often adequate approximation. The two-mass system considered in this thesis is an electrical motor connected to a load with a coupling, as was shown in Fig. 2.1. The simplification is done so that all the inertial effects are located at the motor and the load discs and all the flexibility is located at the coupling. In this thesis the motor and the load are referred with subscripts m and l, respectively. The resonance and the anti-resonance frequencies of a two-mass system can be found as

$$f_{\text{res}} = \frac{1}{2\pi}\sqrt{k_{\text{t}}\frac{J_{\text{m}}+J_{\text{l}}}{J_{\text{m}}J_{\text{l}}}}, \quad (2.4)$$

$$f_{\text{ares}} = \frac{1}{2\pi}\sqrt{\frac{k_{\text{t}}}{J_{\text{l}}}}, \quad (2.5)$$

where the J_{m} and J_{l} are the motor and load inertia, respectively (Saarakkala and Hinkkanen, 2015). The transfer function of a two-mass system from torque to speed is defined as

$$G(s) = \frac{B(s)}{A(s)}, \quad (2.6)$$

where

$$\begin{aligned} B(s) =& J_{\text{l}}s^2 + (c_{\text{t}} + b_{\text{l}})s + k_{\text{t}} \\ A(s) =& J_{\text{m}}J_{\text{l}}s^3 + (J_{\text{m}}c_{\text{t}} + J_{\text{l}}c_{\text{t}} + J_{\text{l}}b_{\text{m}} + J_{\text{m}}b_{\text{l}})s^2 \\ &+ (J_{\text{m}}k_{\text{t}} + J_{\text{l}}k_{\text{t}} + c_{\text{t}}b_{\text{m}} + c_{\text{s}}b_{\text{l}} + b_{\text{m}}b_{\text{l}})s \\ &+ k_{\text{t}}(b_{\text{m}} + b_{\text{l}}), \end{aligned} \quad (2.7)$$

where b_{m} and b_{l} are the friction coefficients of the motor and the load, respectively (Saarakkala and Hinkkanen, 2015).

2.2 Excitation sources

The excitation for the torsional vibrations can be mechanical or electrical. For all rotating mechanical elements there is a possibility of generating oscillating components to the torque spectrum. An unbalance on the blades of an impeller or ellipticity of gears, are of typical examples. The amplitude of the vibration is dependent on the internal damping; low torsional resonances are less damped than the higher ones and hence they are usually of more interest (Niiranen, 2000). Usually the issues are particularly related to the first mode of the torsional vibration. The most severe excitations resulting from an electrical machine are due a short circuit at the machine terminals and are located at the frequencies of one and two times the supply frequency (API 684, 2005). In addition to above, in VFD applications more excitation sources are present due to the harmonics produced in AC-DC-AC conversions. The ripple of the rectified DC-voltage in combination with the inverter characteristics creates fluctuating torque components. The magnitude depends on the frequency converter's structure, e.g. voltage source inverter (VSI) or current source inverter (CSI), as harmonic or inter-harmonic distortion. The main sources are the harmonic content in VSIs whereas the inter-harmonic content are more prudent in CSIs (Mauri et al., 2016). The harmonic and inter-harmonic excitation frequencies produced by VFD can be calculated as

$$f_{\mathrm{exc}} = |n f_{\mathrm{out}} + m f_{\mathrm{in}}|, \tag{2.8}$$

where the n is a positive integer, the m is a positive or negative integer, the f_{out} is the output frequency of the frequency converter and the f_{in} is the input frequency of the frequency converter (Holopainen et al., 2013). For harmonic excitations the m = 0. The n is related to the number of pulses in the inverter and its multiples which typically is 6. According to (Holopainen et al., 2013) the main harmonic excitations can be found with (2.8) when n = 0, 6 or 12 and m = 0 and the main inter-harmonic excita-

tions when n = 0, 6 or 12, and m = -2 or -6.

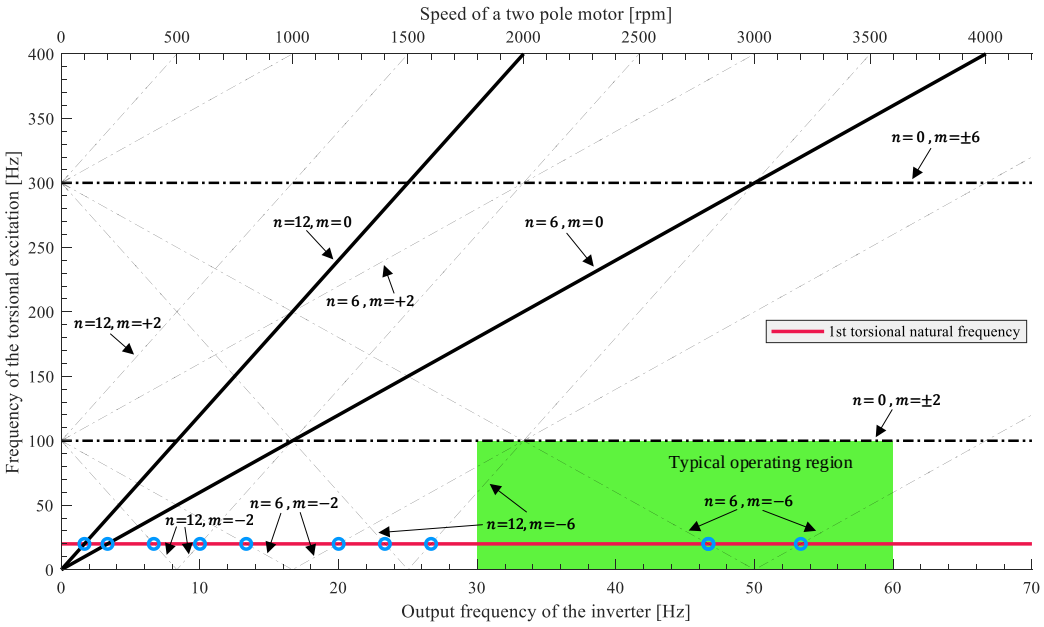

Figure 2.3: An example of a Campbell diagram of the main torsional excitation frequencies of a VFD when the supply frequency of the VFD is 50 Hz. The first torsional natural frequency is shown with the red horizontal line and the interference points are marked with blue circles. The two interference points in the typical operating region should be analyzed if the damping is sufficient.

Usually the natural frequencies and their potential excitation sources are presented using a Campbell diagram. In the diagram, the torsional resonance frequencies are shown as horizontal lines. The interference points can be examined from the diagram from the intersections of the excitation lines and the resonance frequency line. The diagram can be used to detect which excitation sources are present at the operating speed region of the system. If interference point is in the operating region a damped analysis can be carried out to determine if the damping is sufficient enough that the interference can be considered negligible (Corbo and Malanoski, 1996). At the design phase the potential excitation sources could be eliminated or moved. A general Campbell diagram showing the main excitation frequencies of a VFD is shown in Fig. 2.3. Only the first torsional nat-

ural frequency is shown in Fig. 2.3 since it is usually the most crucial one. However, the interference of the higher natural frequencies could also be shown. Although the interference points shown in the operating region might be bigger issue it should be noted that the lower ones are still present during acceleration and deceleration.

2.3 Effects to mechanics

Torsional vibrations can have a major influence to the mechanical system for instance resulting in possible mechanical faults. However, in most cases the torsional vibrations are hard to detect from the shaft train without special instruments and personnel. This might lead to a problem where the torsional stresses continue to be excited until breakage of the coupling or the shaft. Other typical issues are worn gears and cracked gear teeth. Although, sometimes the clattering of gear teeth could also be an indication of the presence of the torsional interference. Moreover, in geared systems the torsional vibration can also create lateral and axial vibrations which could lead to additional damage on the axle (Friswell et al., 2010). Failure at any point of the shaft train could lead to a long shutdown of the plant. It is stated in (Dimarogonas et al., 2013) that a cracked rotor has lower torsional vibration natural frequencies. The uncontrolled or undetected torsional vibrations lead to shorter maintenance intervals and reduced accuracy whereas by monitoring of the resonance frequencies the wearing of the shaft components could be detected. The maintenance could then be ordered and unnecessary plant shutdown duration could be minimized.

2.4 Compensation and detection methods

In the industry, the torsional modes are well known issue of the mechanical train. In addition to the mechanical solutions to damp these vibrations, electrical mitigation techniques have also been developed. Typically the damping algorithms can be integrated to the control loop of the motor. Naturally, in most cases the location of the torsional resonance frequency must be known. In many commercial VFDs the torsional resonances, or so called critical speeds, can be defined to the control software.

The VFD avoids these critical speeds by quickly accelerating past them. In (Schramm et al., 2010) an external torsional mode damping controller is presented to actively decrease the torsional oscillations. The general principle of this method is to sum up the torque reference, from e.g. the speed controller, and a phase shifted torque component to gain a similar damping effect to an increased mechanical damping. A similar oscillation damping method is implemented in a commercial ABB ACS880 frequency converter (ABB, 2019). Generally, if the location of the resonance is known a notch filter is a viable option.

It is noted, that all the methods mentioned above require some external sensors or detailed knowledge of the drive train in question. However, with cost-reduction in mind the sensorless commissioning and operation of a VFD system has been a subject of interest in the industry. For example, a sensorless auto-tuning procedure of a PI controller is presented in (Weber et al., 2014). A sensorless detection of the torsional resonance frequency and speed dependent oscillations is carried out by empirically obtaining the Campbell diagram of the system from multiple measurements (Orkisz and Ottewill, 2012). In the paper, the resonance frequency is also extracted from the speed signal by averaging from multiple different measurements with varying operation conditions. Sensorless frequency response identification is studied using Luenberger adaptive speed observer structure in (Zoubek and Pacas, 2011, 2017) where speed estimate is obtained using the presented observer. The frequency response of the mechanics is obtained between the torque producing current component I_q of the VFD's current measurement and the estimated speed.

3 System identification

Typical control law applied for mechanical or electrical system requires adequate enough plant model which represents the system's dynamic characteristics. In the case of a complex higher order systems, the model is usually approximated to the operating region for the desired application in consideration for simpler control and modeling purposes. With accurate control of a system a reliable and energy efficient performance and longer life time can be achieved. It is obvious that to obtain accurate control the model's structure and parameters must be known or calculable. Sometimes the parameters are unknown or they can change over time in which case system identification approaches are required.

Identification process usually starts by acquiring useful data about the system. This can be done by exciting the system with a known external signal containing frequencies of interest. In some cases the system's natural vibrations may be high enough for that but usually an artificially generated external signal yield to more accurate results (Pintelon and Schoukens, 2001). The next step would be to choose a model structure which can be roughly divided to non-parametric or parametric models. It's always a question of the application if the parametric model is needed. Benefits of the non-parametric identification is that the quality of the data can be visually confirmed in an earlier stage of the process. However, the fitting algorithms used in the parametric identification often use the non-parametric estimate to minimize the error between the selected parameters. This of course means that the parameter estimation problem itself is more complicated process than obtaining the non-parametric estimate and usually requires more insight of the system to choose proper parameter candidates. Lastly the identified model should be validated to confirm that it is a good enough representation of the real system for the application. (Pintelon and Schoukens, 2001)

Identification can be carried out in time or frequency domain. The basic time domain methods usually rely on impulse response or step response analysis. The frequency domain is often preferred since it provides a clear visualization of the system dynamics, such as resonances and model or-

der (Isermann and Münchhof, 2011). Disadvantages are mainly increased computational effort, namely due to time-frequency domain transformations, which can be mainly problem for online identification in the case of limited calculation resources. (Nevaranta, 2016).

Depending on the application the input and output must be chosen accordingly. When identifying the mechanical part of a mechatronic system, a natural choice for input and output would be the shaft torque and the process' output speed, respectively (Saarakkala and Hinkkanen, 2015). Usually, in order to obtain the frequency domain representation of the input and output the discrete Fourier transform (DFT) is used. Generally, the estimated transfer function of the mechanics can then be calculated with

$$\hat{G}(\mathrm{j}\omega) = \frac{\mathrm{DFT}(y(k))}{\mathrm{DFT}(u(k))}, \tag{3.1}$$

where $u(k)$ and $y(k)$ are the discrete measurements of the input and output, respectively (Weber et al., 2014). For practical reasons the closed-loop identification approaches are usually required (Wahrburg et al., 2017). The closed-loop approaches are generally divided to indirect and direct identification (Saarakkala and Hinkkanen, 2015; Ljung, 1987). In the direct approach the input and the output signals used for the identification are measured and the model approximation is calculated similarly as in (3.1). The measured input signal is combination of the excitation signal and the controller output. In the indirect approach only the output signal is measured while the input signal is the known excitation signal. It should be noted that with indirect approach the input and output signals provide information on the closed-loop system. To identify the original system the controller must be known so that it could be extracted from the closed-loop model. (Saarakkala and Hinkkanen, 2015) The identification setup for the indirect and direct approaches can be seen in Fig. 3.1, where the dashed lines show the measured (or otherwise known) signals.

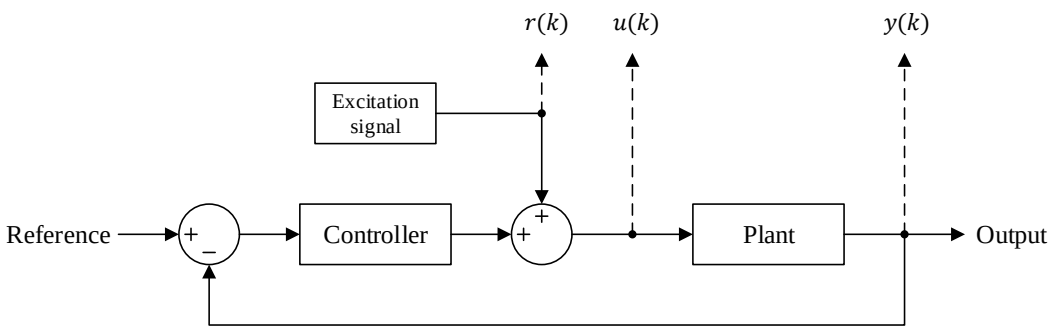

Figure 3.1: A general setup for an indirect or a direct identification of the plant. In the indirect approach the used signals would be the $r(k)$ and $y(k)$, whereas in the direct approach the used signals would be $u(k)$ and $y(k)$.

3.1 Excitation signals

As stated before an external signal is recommended for the system's excitation to obtain accurate results. In system identification applications the basic idea for the excitation signal is to have an adequately rich signal, meaning that frequencies of the desired band must be excited with sufficient amplitude and resolution. With a proper excitation signal the frequency response of the system can be obtained. Often, in the case of simple systems the resonance frequency can be observed from the response without further signal processing. Naturally the power spectrum of the excitation signal, which tells how the signal's power is distributed on the frequency domain, depends on multiple factors so it must be designed accordingly for the specific application.

In the non-parametric identification it's more significant to have a well designed excitation since the system is represented using the measured signals (Pintelon and Schoukens, 2001). The goodness of an excitation signals can be compared generally with two factors; crest factor and time factor. The crest factor is defined as the ratio of the peak and the RMS value of the signal. This means that an excitation signal with a low crest factor has the power more evenly distributed than with high crest factor. The time factor specifies how long measurement is required to obtain a sufficient sig-

nal to noise ratio. (Schoukens et al., 1988; Pintelon and Schoukens, 2001)

There are multiple well-established excitation signals used in identification routines. It is highly recommended to use periodic excitation signals since this reduces the leakage effect of the DFT as well as the measurement time (Pintelon and Schoukens, 2001). Commonly used periodic signals are swept sine, multisine and pseudo-random binary sequence (PRBS). The swept sine, or chirp signal, is a signal where a sine wave is swept through the desired frequency range up or down in given time window (Vuojolainen et al., 2017). With this it's possible to accurately specify the frequencies to be excited without increasing disturbances on the non-relevant frequencies. However, the swept sine usually requires relatively long measurement time as can be seen from Table 3.1. The multisine signal consists of multiple sine signals with carefully chosen frequencies and amplitudes. One advantage is that the power can be focused directly on the frequencies that provide the most information of the system. The PRBS is a signal that varies between two values at multiples of the generating clock frequency. The PRBS is said to be an approximation of white noise on the effective frequency band which enables the generation of a wide band signal with even spectral content (Corriou, 2004). The generation of the PRBS signal and its properties are discussed below in more detail.

The design of the excitation signal is often a compromise between the accuracy and measurement time. In most cases the only physically limiting factor is the amplitude (Pintelon and Schoukens, 2001). However, in more complicated applications, such as the active magnetic bearings, the excitation signal must be designed more carefully (Hynynen, 2011). The basic properties of the discussed excitation signals are presented in Table 3.1. It is worth mentioning that in this thesis only the PRBS excitation signal is used for the identification.

3.1.1 Pseudo-random binary sequence

In literature, the PRBS is commonly recommended excitation signal for a wide band examination of the system. One of the key benefits of the PRBS

Table 3.1: Typical properties of excitation signals according to (Pintelon and Schoukens, 2001). The values are for general purpose signals and could be improved by optimizing them for the process in question.

Signal	Crest Factor	Time factor
Chirp	1.45	1.5-4
Multisine	1.7	1.5
PRBS	1	1.5

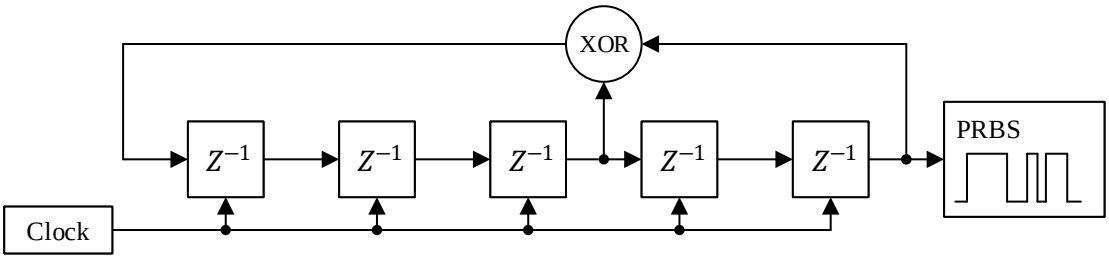

Figure 3.2: The PRBS generation with five shift registers and a XOR gate. The Z^{-1} is a unit delay.

is that it's easy to generate since it only has two values A or $-A$, where A is the amplitude. The generation of the PRBS can be implemented efficiently with shift registers and feedbacks, see Fig. 3.2 where example generation of the signal is shown. (Pintelon and Schoukens, 2001).

The design variables for maximum length PRBS are the desired bandwidth f_{bw}, length of the period N, the amplitude A, the generating frequency f_{gn} and the sampling frequency f_{s} (Vilkko and Roinila, 2008). In some cases some variables might be limited for practical reasons, for example, the number of registers available, the sampling frequency or the number of samples. A good starting point for the PRBS design is to define the minimum period for the PRBS which must be at least the settling time of the process to avoid time aliasing (Vilkko and Roinila, 2008). The generating frequency is suggested to be about 2.5 times the bandwidth of interest (Pintelon and Schoukens, 2001). Knowing the f_{gn} and the duration of one period T of the PRBS the minimum length and the number of registers can be determined as

$$N = 2^h - 1 \geq f_{\text{gn}} \cdot T, \tag{3.2}$$

where h is the number of registers. However, by increasing the number of registers, a better frequency resolution can be obtained. The frequency resolution can be calculated with (3.3) (Mohammed et al., 2019).

$$f_{\text{r}} = \frac{f_{\text{gn}}}{N}. \tag{3.3}$$

The sampling frequency f_{s} is recommended to be at least 4 times the generating frequency to capture frequency content of the PRBS (Vilkko and Roinila, 2008). The number of samples needed to save one period of data can be calculated with (3.4) (Vuojolainen et al., 2017).

$$L = \frac{N \cdot f_{\text{s}}}{f_{\text{gn}}} = \frac{(2^h - 1) \cdot f_{\text{s}}}{f_{\text{gn}}}. \tag{3.4}$$

A PRBS that has the maximum length with a fixed amount of registers is often referred as maximum length binary sequency (MLBS). To generate a MLBS with a circuit shown in Fig. 3.2, the feedback points must be chosen accordingly. A few possibilities for the feedback positions with different register lengths are shown in Table 3.2. The external noise in the measurements can be reduced by allowing the PRBS to run for multiple number of periods (Vilkko and Roinila, 2008).

A frequency and time domain plots of a PRBS signal, that is generated with a setup like shown in Fig. 3.2, are shown in Fig. 3.3. The period $T = N/f_{\text{gn}} = 3.1$ s can be observed from the time domain plot shown in Fig. 3.3b.

The bandwidth of the excitation signal is advised to keep significantly below the switching frequency of the frequency converter. However, in most cases the torsional natural frequencies are located below 100 Hz and hence the switching frequency is not a limiting factor in this case.

Table 3.2: Register lengths, length of the period and feedback positions that yields to a MLBS (Isermann, 1981).

Number of registers h	Length of the period N	Index of the feedback registers
5	31	3, 5
6	63	5, 6
7	127	4, 7
8	255	2,3,4, 8
9	511	5, 9
10	1023	7, 10
11	2047	9, 11

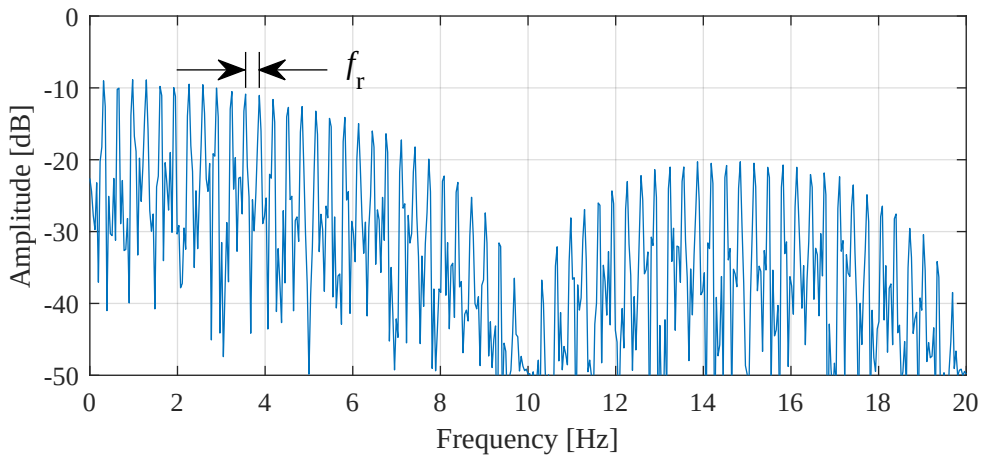

(a)

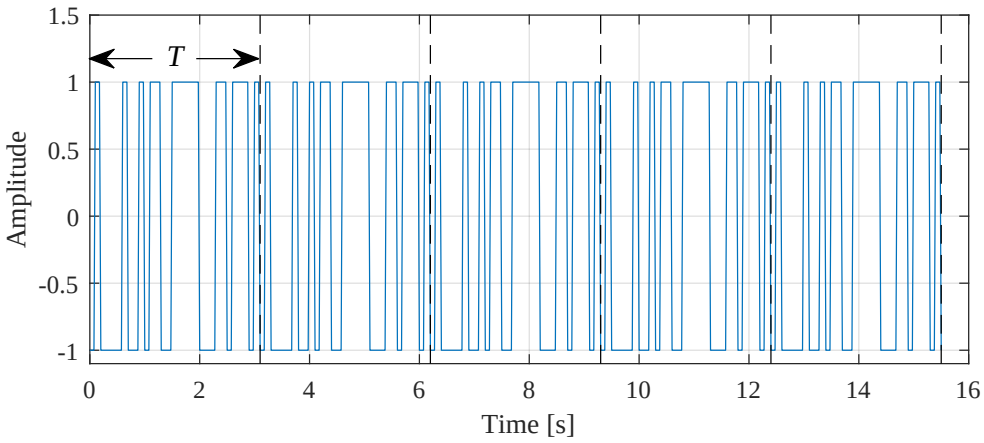

(b)

Figure 3.3: A PRBS signal presented in frequency (a) and time domain (b). The generation is done with a circuit shown in Fig. 3.2 with following parameters: the A = 1, the f_{gn} = 10 Hz, the h = 5, the number of periods = 5, the f_s = 40 Hz. The frequency resolution f_r can be seen in (a). In (b) the periods are separated with dashed lines.

3.2 Spectral analysis

Commonly the measured time domain signals are transferred to the frequency domain using DFT. This is a straightforward method to quickly check the main frequency characteristics of a signal. Typically, in the case of non-parametric identification methods, the DFT is further processed to estimate the power spectral density (PSD). One method to estimate the PSD is called periodogram (Stoica and Moses, 2005). However, the variance of a periodogram is relatively large which is the reason that so-called modified periodograms like Bartlett method and Welch method are typically used which aim to reduce the variance. The difference between basic periodogram and the Bartlett method is that in the latter the analyzed signal is divided to a number of sections for which the periodogram is then calculated. The obtained periodograms are then averaged. On the contrary, the Welch method is an improved version of the Bartlett method where the sections can overlap and they are windowed before calculating the periodograms (Welch, 1967). With windowing, the spectral leakage is also reduced resulting to a more accurate PSD estimate. The equation for the PSD obtained with the Welch method is expressed as

$$\hat{S}_{\mathrm{uu}}(\mathrm{j}\omega) = \frac{1}{SK}\sum_{i=1}^{K}\left(\frac{1}{M}|\mathrm{DFT}(u_i(k_{\mathrm{M}})\cdot w(k_{\mathrm{M}}))|^2\right), \tag{3.5}$$

where K is the number of the sections, the i is the index of the sections, the M is the number of the data points in one section, the k_{M} is a discrete time instant of the section data, the $w(k_{\mathrm{M}})$ is the spectral window and the S is a scaling factor that depends on the spectral window. The complete derivation of the (3.5) can be found in (Villwock and Pacas, 2008).

The Welch method is widely used also in frequency response estimation of a two-mass mechanical systems (Villwock and Pacas, 2008; Saarakkala and Hinkkanen, 2015; Wahrburg et al., 2017). The non-parametric frequency response of the plant shown in Fig. 3.1 can be estimated with

$$\hat{G}(\mathrm{j}\omega) = \frac{\hat{S}_{\mathrm{uy}}(\mathrm{j}\omega)}{\hat{S}_{\mathrm{uu}}(\mathrm{j}\omega)}, \tag{3.6}$$

where $\hat{S}_{\text{uy}}(\text{j}\omega)$ is the Welch's cross power spectral density between $u(k)$ and $y(k)$ and the $\hat{S}_{\text{uu}}(\text{j}\omega)$ is the Welch PSD of the $u(k)$. An accurate parametric identification procedure using a combination of the Welch method and Levenberg-Marquardt algorithm is presented in (Villwock and Pacas, 2008). In this thesis, the discrete time signals are analyzed with the Welch's PSD estimates and the non-parametric frequency responses are estimated using (3.6). The data is divided into eight sections with 50 % overlap and they are windowed using the Hamming window.

4 Closed-loop experimental results

The identifiability of the torsional natural resonance is tested with an experimental setup at LUT laboratory. The setup consists of two asynchronous machines: ABB 7.5 kW machine (M3KP-132SMD-4) on the motor side and ABB 11 kW machine (M3BP-160MLA-4) on the load side. The machines are coupled together with a flexible coupling of which torsional stiffness is a non-linear function of the total load of the system. The used setup is shown in Fig. 4.1a, where the load is located on the left and the motor on the right. The setup can be considered to be a two-mass system since the stiffness of the coupling is much lower than the stiffness of the shafts of the machines. For data validation, two couplings are used that have different stiffness-to-load responses. The used couplings shown in Fig. 4.1b are size 42 ROTEX® 92 Shore A spider and 98 Shore A spider both manufactured by KTR. The torsional stiffness values against the applied torque found in datasheet are shown in Fig. 4.2 (KTR, 2020). It should be noted that the used couplings allow backlash meaning that with lower torques the stiffness becomes undefined. Since the rated torques of the studied machines are at this undefined region the datasheet values can't be used for reference. On the contrary the reference resonance must be identified. The nominal values of the machines are presented in Table 4.1.

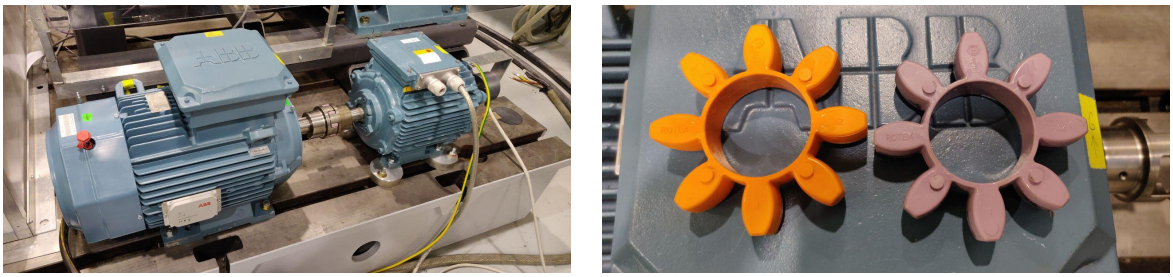

(a) (b)

Figure 4.1: The experimental setup at the LUT laboratory (a) and the used KTR ROTEX® couplings (b) with the 92 Shore A on left and 98 Shore A on right.

4.1 Frequency converter ACS880-01

The both machines are controlled using ABB ACS880-01 frequency converters. The reference values can be entered with programmable logic

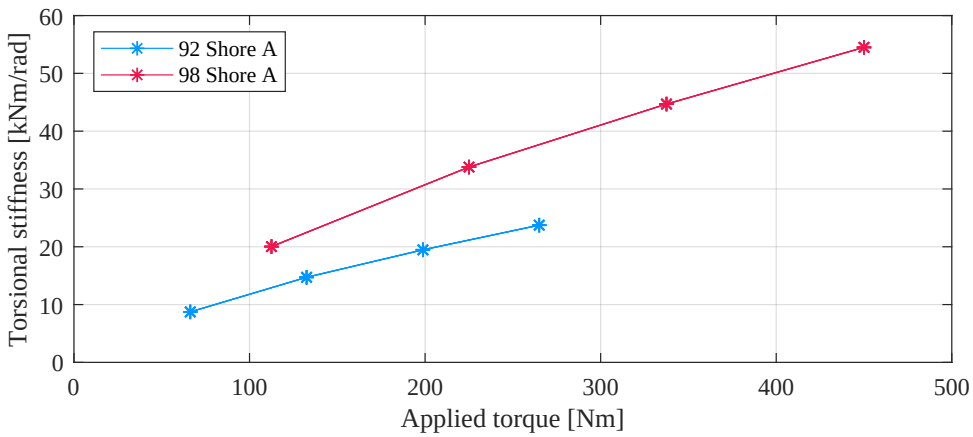

Figure 4.2: The torsional stiffness values of the used KTR ROTEX® couplings against the applied torque according to the datasheet (KTR, 2020).

Table 4.1: The nominal values of the asynchronous machines

Parameter	Motor	Load
Power P_N	7.5 kW	11 kW
Speed n_N	1447 rpm	1473 rpm
Torque τ_N	49.5 Nm	71.3 Nm
Inertia J	0.034 kgm^2	0.103 kgm^2
Frequency f	50 Hz	50 Hz

controller (PLC). The EtherCAT fieldbus is used as the communication network between the ACS880-01 and PLC for which the FECA-01 EtherCAT adapter module is needed. The FECA-01 module allows the external control of the drives. With the FECA-01 module it's possible to control two reference values and feedback two actual values that are selected from the drive's parameter list.

The operation mode of the motor side is set to speed control mode. The speed is controlled with a PI-controller where proportional gain $K_P = 5$ and integration time $T_I = 2.5$ s. The control loop of the ACS880-01 of the motor side is shown in Fig. 4.3. It can be seen that the reference signals for the machine control are coming from the fieldbus adapter (FBA A), the reference 1 being the speed reference. The excitation signal is fed in to the additive torque 2 so the actual torque reference of the DTC is the sum of the speed controller output and the PRBS signal. The collected data to the PLC are the filtered speed (parameter 90.01 Motor speed for control) and

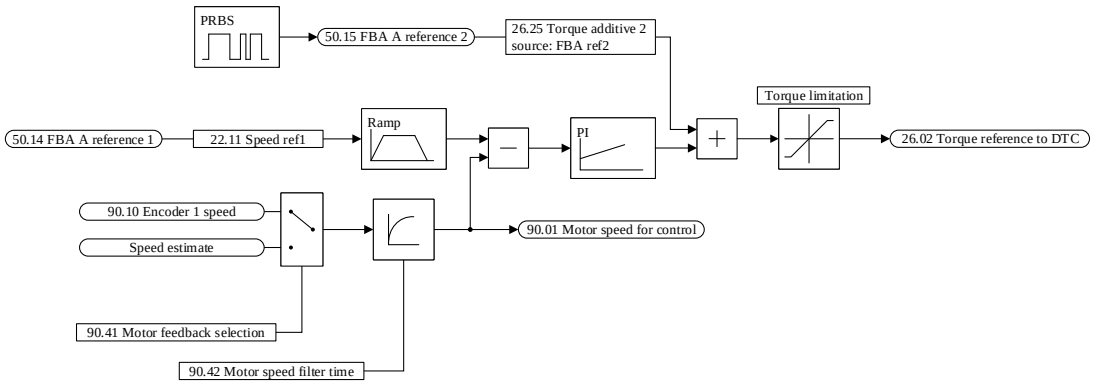

Figure 4.3: The relevant parts of the inner control loop of the ACS880-01 that controls the motor. The numbers are referring to the number of the parameter in the ACS880-01.

the torque reference to DTC (parameter 26.02 torque ref used) as shown in Fig. 4.3. The parameter ”90.42 Motor speed filter time” is set to 0 ms. The actual speed of the motor is measured with an absolute encoder which is connected to the drive with FENA-11 module. For the sensorless identification purposes the feedback selection of the speed control can be set to the speed estimate of the ACS880-01.

The total torque of the system is controlled with the loading machine. The operation mode of the load side is set to torque control mode. The torque reference source for the load is read from the FECA-01 through the fieldbus and it is set with the PLC.

4.2 ABB AC500 PLC and the PRBS generation

The PLC consists of PM583 CPU, CM579 communication module and CD522 IO module. The PLC is used for controlling the speed and torque reference for the motor and load, respectively, as well as the PRBS generation, the start of the identification experiment and data acquisition. The CM579 is used to communicate with the frequency converters while the CD522 is used to output an external trigger signal to a Yokogawa PZ4000 power analyzer which is measuring the motor side three phase stator currents. The control software and the user interface are implemented using ABB Automation Builder 2.1 software.

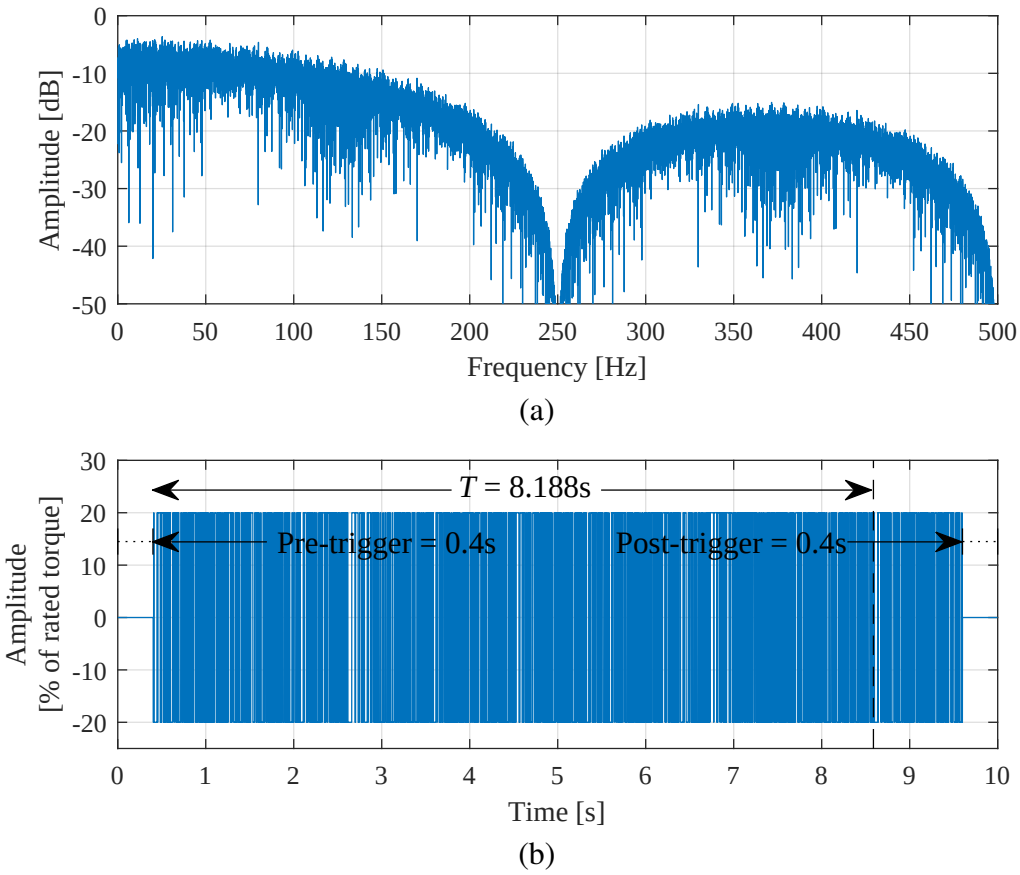

Figure 4.4: The PRBS that was used in the measurements in frequency (a) and time domain (b).

The minimum task cycle for ABB AC500 is 1 ms which limits the maximum sampling frequency to 1000 Hz. To record enough data the PRBS generating frequency is set 4 times lower than the sampling frequency as suggested in Section 3.1.1. With the f_s = 1000 Hz, this results to generating frequency of 250 Hz and bandwidth of about 100 Hz. The PRBS is generated with 11 registers to make sure that the frequency resolution is enough. The samples needed to save one period, according to (3.4), is then 8188 samples. Recording this amount of data takes 8.188 s, however a round 10 s is used to simplify the PRBS generation. A pre-trigger and post-trigger time of 0.4 s is used to accurately record the stator currents from the whole PRBS period. Typically amplitude of 10-25 % of the rated torque is applied in the case of similar mechanical systems (Nevaranta, 2016; Villwock and Pacas, 2008; Saarakkala and Hinkkanen, 2015; Wahrburg et al.,

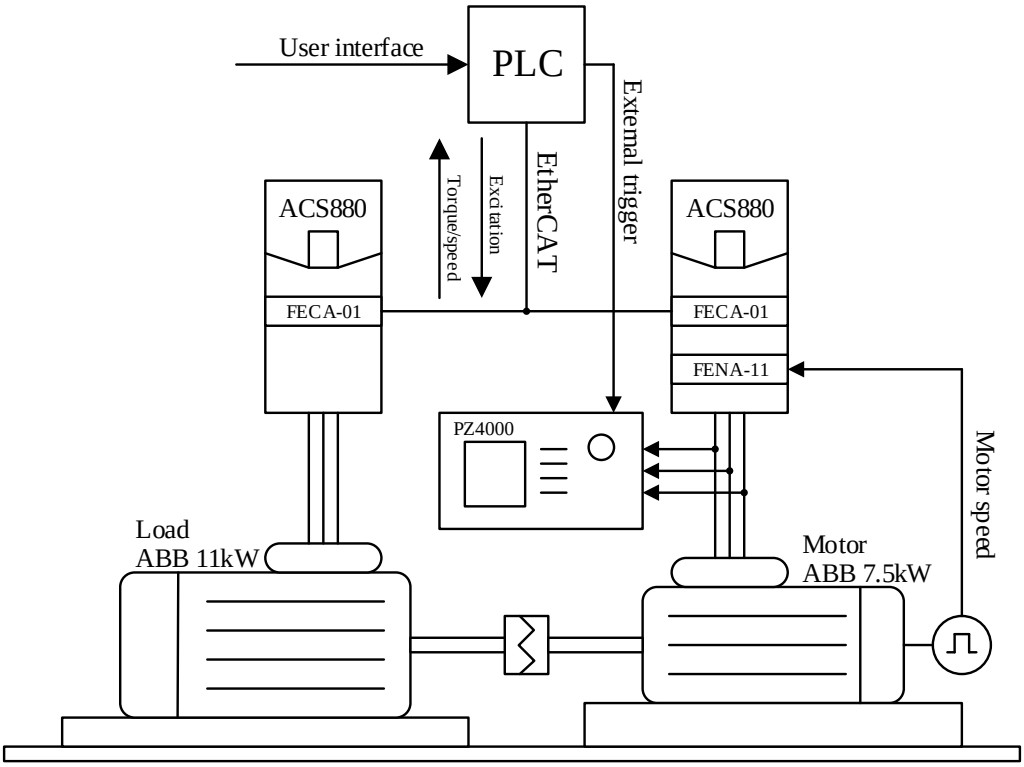

Figure 4.5: The structure of the experimental setup and data acquisition system.

2017). In this thesis the amplitude of 20 % of the rated torque is used. The PRBS frequency spectrum and the whole signal against time are shown in Fig. 4.4. This excitation signal is used in all the measurement cases. The presented experimental setup and data acquisition system is shown in Fig. 4.5.

4.3 Measurements and results

Since the torsional stiffness of the coupling is not known for every load the open-loop frequency response of the mechanical system is first identified using the speed encoder. The machine inertias being constant the stiffness and the damping can be fitted to the identified non-parametric frequency response estimate.

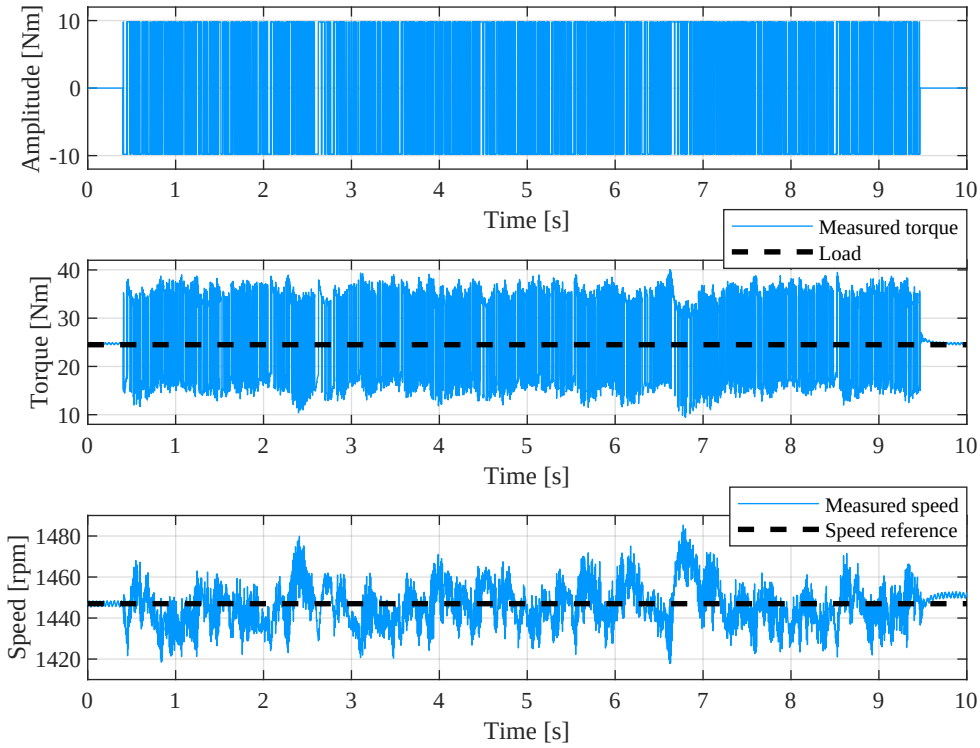

Figure 4.6: The recorded PRBS, torque and speed signals of a measurement case where the PRBS amplitude is 20 % of the rated torque, the load is 50 % of the rated torque and the speed reference is 1447 rpm.

The test is carried out so that the motor is first accelerated to a non-zero reference speed and the load is set to a constant value after which the PRBS is added to the torque reference. An example case of signals recorded by the PLC is shown in Fig. 4.6. The input parameters for the reference case used here are: speed reference 1447 rpm, which is the rated speed, and 50 % rated load. The percentage of the load is set according to the motor's rated torque. The presented results use the ROTEX® 98 Shore A coupling unless otherwise specified. The detection of the torsional vibration is studied by considering two cases for the speed feedback control; I) using encoder as a feedback and II) using the speed estimate of the frequency converter.

The non-parametric frequency response calculated with (3.6) and the estimated theoretical frequency response (2.6) of the reference case are shown in Fig.4.7. The resonance is found at 110 Hz in this case.

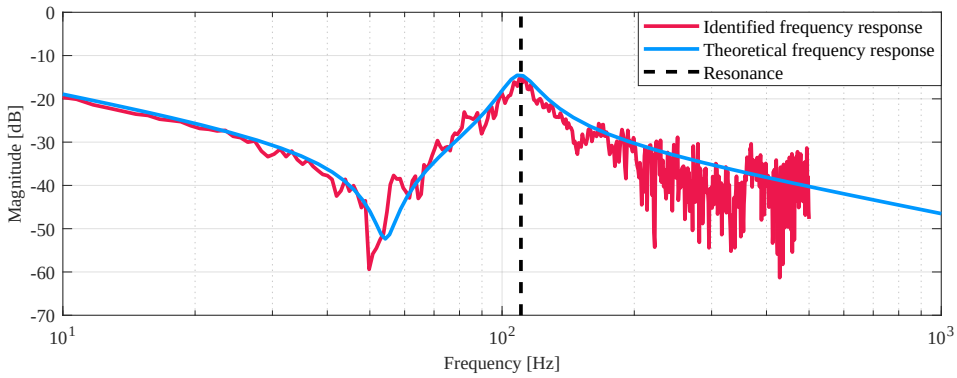

Figure 4.7: The estimated non-parametric frequency response for the case where the speed reference is 1447 rpm and the load is 50 % of the rated torque. The resonance of 110 Hz is found at the peak of the response and is marked with a dashed line.

4.3.1 Torque measurement analysis

The torque signal is analysed by calculating the non-parametric frequency response between the excitation signal and the torque reference. The measurement data for three different load conditions are recorded. The three different loads are 0 %, 25 % and 50 % of rated torque, respectively. As was stated before, the stiffness of the coupling is a function of the load torque meaning that the resonance frequency is different for the three cases. The obtained frequency responses for the measured and sensorless approaches are shown in Figs. 4.8a and 4.8b, respectively. As can be seen with the encoder, there is a negative peak at around the location of the resonance frequency in all three cases. The resonance is assumed to be found at the lowest point of the peak. Compared to the responses obtained with the encoder, the resonance from the sensorless approach is offset about 20 Hz in the loaded cases. However the no-load case is somewhat accurate. However, the method is questionable since it's not so clear where the resonance should be observed even with the measured case as can be seen from the 50 % load case. Nonetheless, some indication of the location of the resonance can be found. During the experiments it was also noticed that the peak was not visible with poorly designed speed controller.

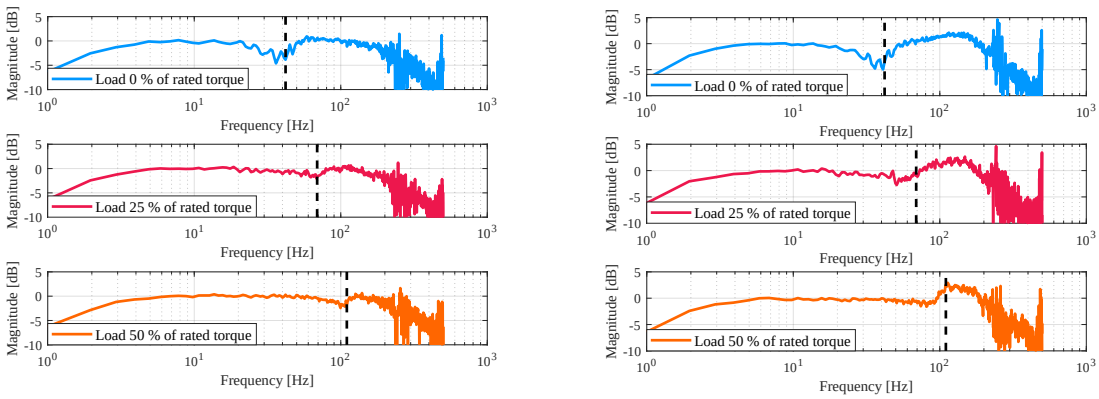

(a) (b)

Figure 4.8: The estimated PRBS to torque frequency response with three different loads for the cases where the speed feedback is from (a) the encoder and (b) the estimator. The resonance frequency shown with the dashed line is estimated similarly to the case shown in the Fig. 4.7. The resonances for the three cases are 42 Hz, 69 Hz and 110 Hz.

4.3.2 Speed measurement analysis

The recorded speed signals with the same load conditions as before are analysed. The most evident results were obtained with the Welch PSD of the speed. The Welch PSD of the measured speed for the three different loads with the encoder and encoderless approach are shown in Figs. 4.9a and 4.9b, respectively. The resonance can be seen very clearly at the peak of the frequency spectrum. The negative peak before the resonance is most likely result of the mechanical antiresonance. It's worth noting that the resonance can be accurately observed from the drive's speed estimate without any sensors as can be seen from the Fig. 4.9b. However, the peak seems to become more evident with higher loads.

4.3.3 Current measurement analysis

As mentioned before, the three phase stator currents were measured with Yokogawa PZ4000 power analyzer so this section does not directly present solution for detection of the resonance with the VFD itself. The Welch PSD of the motor's phase A current with and without the PRBS are shown in Fig. 4.10. The only noticeable peaks are due to rotational speed of the motor, harmonics and switching frequency. The conclusion is that the resonance can't be seen in the stator reference frame in the closed-loop case.

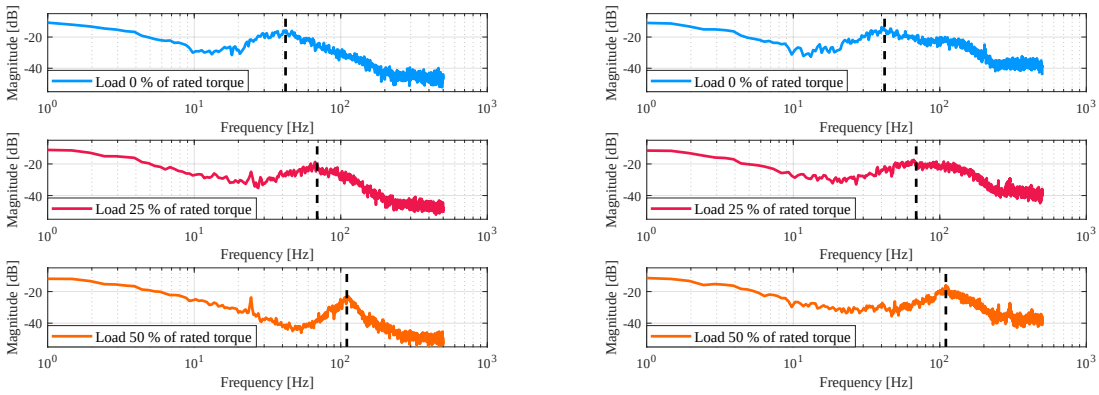

(a) (b)

Figure 4.9: The Welch's power spectral density estimate of the speed signal with the speed feedback from (a) the encoder and (b) the estimator

The currents were also analyzed in the rotor reference frame since torque producing component, i_{q}, should show similar results as in Section 4.3.1. To transform the currents to dq-reference frame the rotor position was estimated with phase locked loop (PLL) from the measured three phase currents. In Fig. 4.11 are shown the estimated i_{d} and i_{q} against time. The pulses of the used PRBS are clearly visible in the estimates.

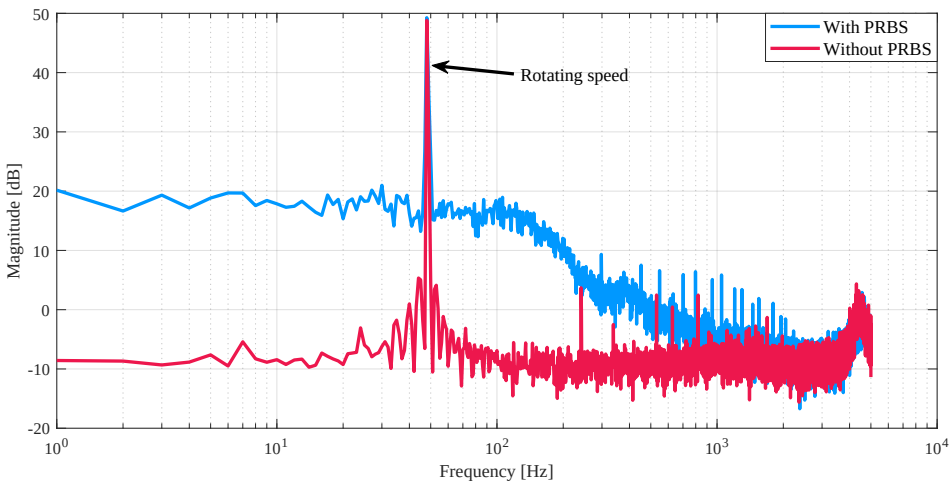

Figure 4.10: Welch PSD estimate of the motor phase A current with and without the PRBS. The PRBS bandwidth of 100 Hz is clearly visible.

The estimated i_{d} and i_{q} were analyzed in the frequency domain with the

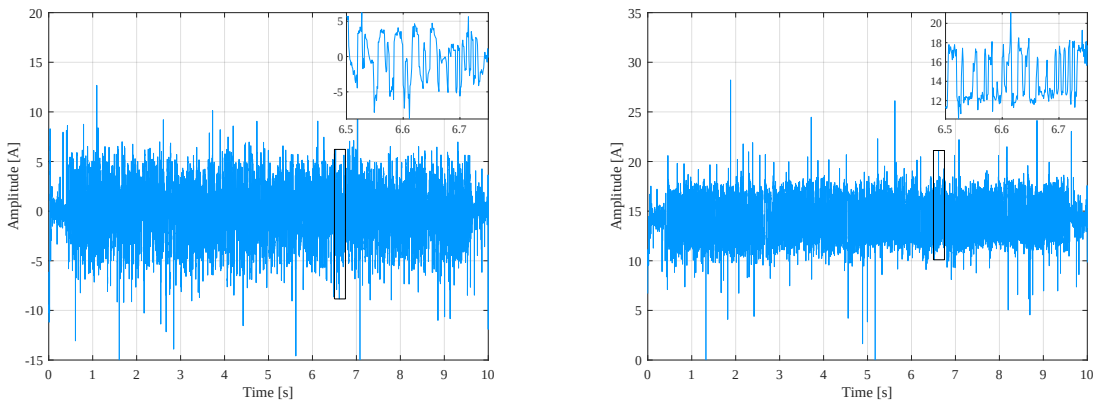

(a) (b)

Figure 4.11: Estimated rotor reference frame currents i_d (a) and i_q (b).

Welch PSD and the frequency response between the excitation signal and the current component estimated with the Welch method. The frequency response from the PRBS to the estimated i_d and i_q for two couplings are shown in Figs. 4.12a and 4.12b, respectively. In Fig. 4.12a a negative peak can be seen around the actual resonance for both couplings with this particular case where the speed reference is 1447 rpm and the load is 50 % of the rated torque. With the softer coupling a negative peak can also be seen in Fig. 4.12b. However, with lower load conditions the frequency responses don't show similar results. This might be a cause of a poor rotor position estimator and hence poor i_d and i_q estimates. The fact that with lower load conditions the PRBS was not as clearly seen in the i_d or i_q as in Fig. 4.11 would refer to this. Another possibility is that the negative peaks shown in Fig. 4.12 are a result of some other factor than the mechanical resonance. The experiments show that the maximum value at around 30 Hz in Fig. 4.12a is due to the rotational speed and around that the shape of the response remains somewhat the same for the different loads. This means that the rotational speed needs to be low enough so that the maximum value shown in the frequency response is below the resonance. This leads to that if the resonance is located at relatively low frequency this method might not be the best alternative to detect that. This method of detecting the mechanical resonance from the frequency response between the PRBS and the current component would need more thorough studying with more measurement points with different load conditions, reference speeds and

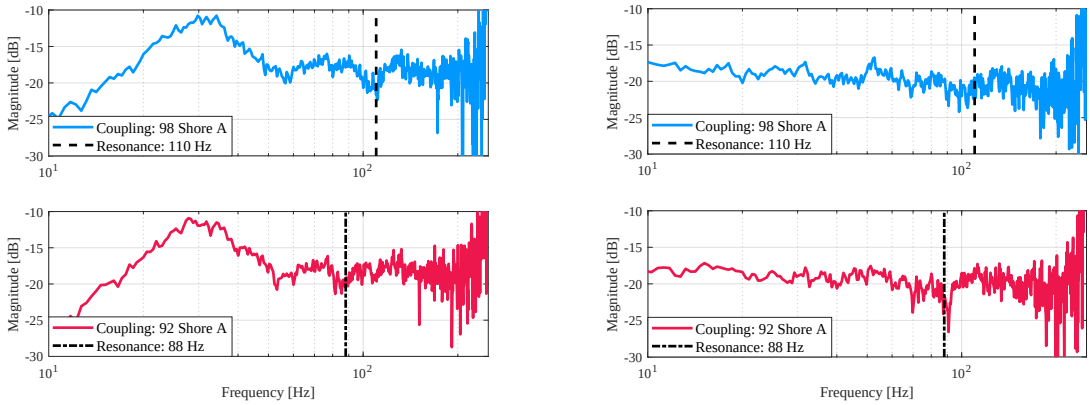

(a) (b)

Figure 4.12: The frequency response for two couplings (a) between the PRBS and the estimated i_d and (b) between the PRBS and the estimated i_q.

excitation signals. Furthermore, it should be investigated what components cause the shape of the frequency response between the PRBS and the i_d.

4.4 Discussion

In this chapter the identifiability of the torsional natural frequency of a VFD system using motor's torque, speed and current signals were tested experimentally. The goal was to find out if the signals that are obtainable from a commercial frequency converter could be used to detect the first torsional natural frequency without additional sensors. The signals were analysed in frequency domain with Welch's method for obtaining the PSD or frequency response estimates between different signals. The plant was excited with a known PRBS signal. First, the location of the actual resonance frequency was identified from the estimated frequency response between the torque reference of the VFD and the measured rotational speed. The signals were analyzed first with the encoder feedback to find out if the resonance frequency could be identified with the studied methods. The speed feedback was then changed to the drive's speed estimator to test the applicability to the sensorless identification. From the studied signals, the resonance frequency could be detected from the torque and the speed. The current signal would have needed more advanced signal processing and more thorough analysis. Due to limited resources the current signal analy-

Table 4.2: Estimated resonances from the torque and speed signals with and without the encoder for two couplings with different hardness.

			Encoder		Estimator	
Load	Coupling	Reference resonance	Torque	Speed	Torque	Speed
0 %		42 Hz	41 Hz	41 Hz	40 Hz	41 Hz
25 %	98 Shore A	69 Hz	68 Hz	67 Hz	51 Hz	66 Hz
50 %		110 Hz	106 Hz	111 Hz	92 Hz	110 Hz
0 %		35 Hz	33 Hz	33 Hz	32 Hz	36 Hz
25 %	92 Shore A	64 Hz	65 Hz	63 Hz	57 Hz	64 Hz
50 %		88 Hz	91 Hz	88 Hz	82 Hz	91 Hz

sis were carried out only to some extent. In addition, the experiments show that the resonance frequency could be identified from the speed signal with quite minimal signal processing so the more demanding analysis was considered unjustified.

A summary of the estimated resonance frequencies are shown in Table 4.2. As can be seen the drive's speed estimator shows the most promising results. With the sensorless identification from the speed signal, the error of the estimated resonance frequencies are < 5 % for the tested cases. An important remark is that the reference resonance is also just an estimation. However, the identified frequencies with the encoder are showing similar results so it is considered to be reasonably accurate.

As mentioned before, the characteristics of the couplings are usually dynamic and non-linear. This can be seen from the results where the resonance rises as the load gets higher. In this thesis, the non-linear effects are emphasized with the smaller loads since the PRBS amplitude is higher than the static load torque. Due to this the torque of the motor is transitively negative which increases the effects of the backlash. With this in mind, when considering the application for the proposed methods, it should be noted that the identified resonance for a no-load case might not be applicable at the actual operating point of the drive. However, in some cases it's useful to identify the resonance characteristics for varying loads. Another remark is that the proposed methods are carried out as a one time ID-experiment. Therefore the applicability for a continuous monitoring purposes should be studied in more detail. It is clear that the amplitude of the excitation

signal in such case should be significantly lower than the 20 % of the rated torque used in this thesis. Likewise, for the ID-test application the amplitude should be minimized.

5 Direct on line application

In this chapter a simulation model is presented to simulate a direct connected induction motor. The purpose of the simulations is to find out if the resonance frequency of the mechanical system can be observed from the stator current of the motor in the direct on line (DOL) applications. The simulated cases are also experimentally tested in LUT laboratory.

5.1 Simulation model and results

The simulation model is build using MATLAB Simulink®. The induction motor is direct connected to a 400 V 50 Hz grid. The simulation model is shown in Fig. 5.1. The mechanical model of the two-mass system used in the simulation is shown in Fig. 5.2. The rotor friction coefficients, b_{m} and b_{l}, are included in the model as a viscous damping for both the motor and the load, respectively. The electrical parameters for a same size motor as in the laboratory are used for the induction machine model. The electrical parameters of the induction motor and the parameters of the mechanical model are given in Table 5.1.

Table 5.1: The electrical parameters of a 7.5 kW 400 V 50 Hz 1440 rpm induction motor and the initial mechanical parameters that were used in the simulation.

Electrical		Mechanical	
Parameter	Value	Parameter	Value
Stator resistance R_{s}	0.7384 Ω	Motor inertia J_{m}	0.034 kgm^2
Stator leakage inductance $L_{\mathrm{s}\sigma}$	3.045 mH	Motor friction b_{m}	0.005 Nm·s/rad
Rotor resistance R'_{r}	0.7402 Ω	Load inertia J_{l}	0.103 kgm^2
Rotor leakage inductance $L'_{\mathrm{s}\sigma}$	3.045 mH	Load friction b_{l}	0.005 Nm·s/rad
Magnetizing inductance L_{mag}	124.1 mH	Torsional stiffness k_{t}	$7.8 \cdot 10^3$ Nm/rad
Pole pairs p	2	Torsional damping c_{t}	3 Nm·s/rad

As shown in Fig. 5.1, the PRBS is now superposed to the load torque. This due to experimental system where the load side drive is used to generate excitation to the system in order to identify the flexible behavior by measuring the grid side machine currents. The frequency response of the mechanical model can be estimated from the load side with the Welch method

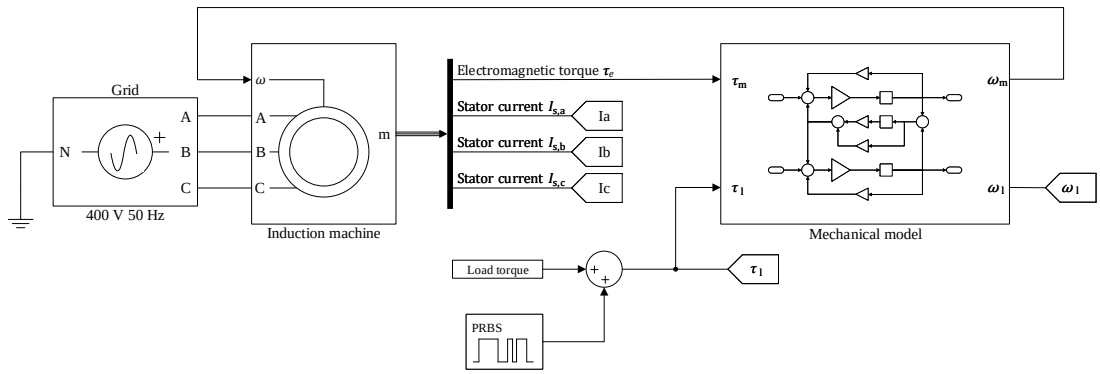

Figure 5.1: A representation of the Simulink® model. The mechanical model is shown in Fig. 5.2 in more detail.

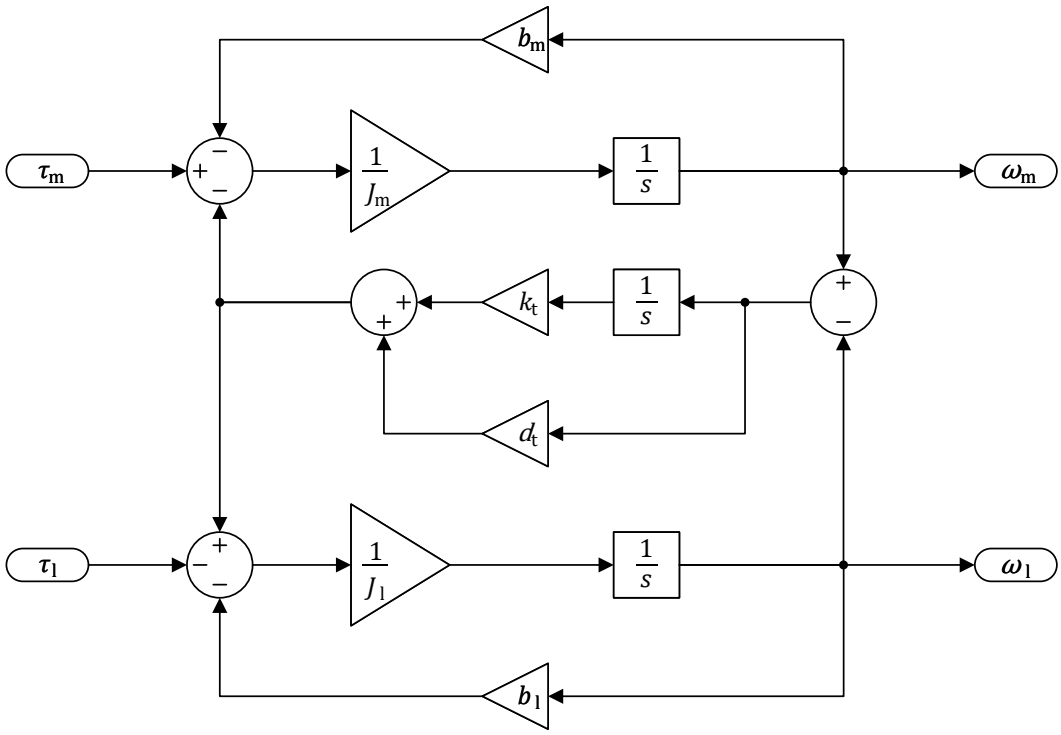

Figure 5.2: The mechanical model of the two-inertia system, where the τ is the electromagnetic torque, b is the friction coefficient, ω is the angular velocity. The subscripts m and l are representing the motor and the load, respectively.

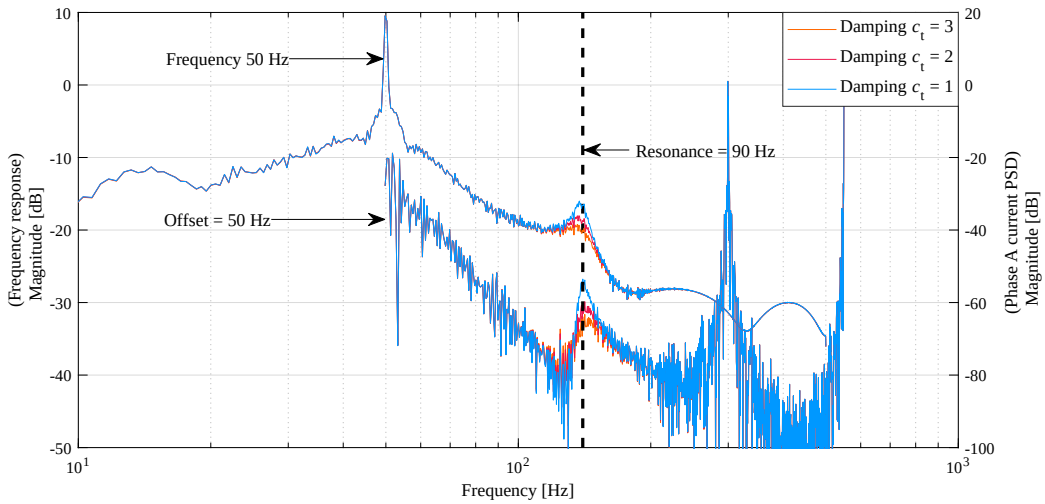

Figure 5.3: The frequency response of the mechanical model estimated with the Welch method (left y-axis) and the Welch PSD of the phase A current of the induction motor (right y-axis) from the simulation of varying torsional damping. The used PRBS amplitude is 20 % of the rated torque.

from τ_l to ω_l. The load torque is set to 50 % of the rated torque. The PRBS signal used in the simulation is the same as the one used in Chapter 4 with amplitude of 20 % of the rated torque. The simulation is carried on for three different torsional damping values. The frequency response of the mechanical system estimated with the Welch method and the Welch PSD of the Phase A current are shown in Fig. 5.3. The resonance of 90 Hz is observed from frequency response where the $c_t = 1$ and is shown with the dashed line. The frequencies of the frequency response and the resonance are offset by 50 Hz, which is the supply frequency of the motor. The resonance can be observed from the current PSD at $f_{in} + f_{res}$. It can be seen that with lower damping the resonance can be seen more clearly from both, the current PSD and the frequency response. Fig. 5.4 shows that increasing the PRBS amplitude does not improve the observability of the resonance from the current PSD. However, the distortion of the frequency response decreases. One important remark should be emphasized; the studied simulation is ideal as there is no noise sources or non-idealities included that have an influence to the results.

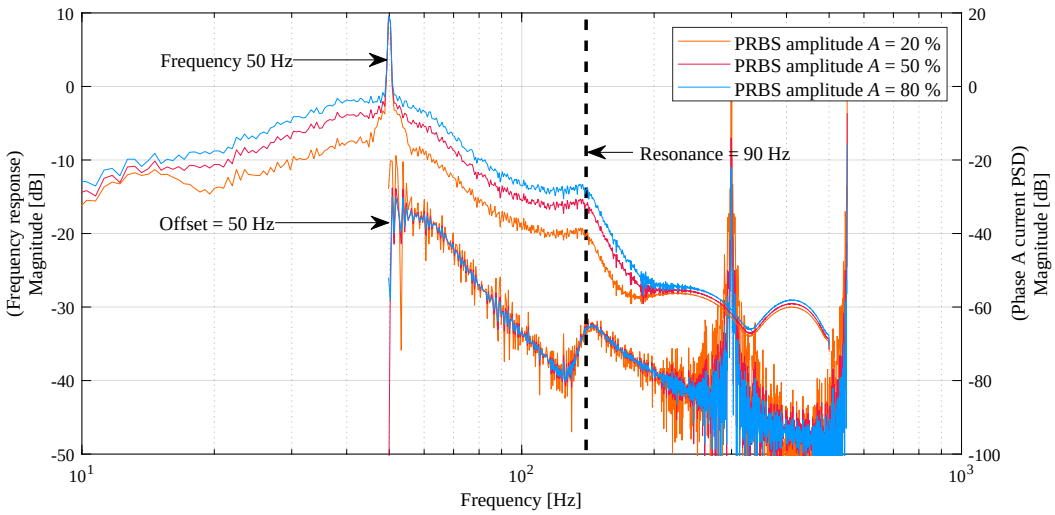

Figure 5.4: The frequency response of the mechanical model estimated with the Welch method (left y-axis) and the Welch PSD of the phase A current of the induction motor (right y-axis) from the simulation of varying PRBS amplitude. The used PRBS amplitudes are 20 %, 50 % and 80 % of the rated torque and the torsional damping c_t is 3 Nm·s/rad.

5.2 Experimental results

The experimental setup presented in Chapter 4 is modified so that the motor is supplied directly from the 400 V 50 Hz grid. As in the simulations, the PRBS is now superposed to the load torque. The load torque and the PRBS amplitude are set to 50 % and 20 % of the rated torque, respectively. The Welch PSD of the measured phase A current and the frequency response estimated with the Welch method are shown in Fig. 5.5. The measurements for the frequency response were carried on with the setup presented in Chapter 4 where the load was 50 % of the rated torque and the used coupling was the KTR ROTEX® 92 Shore A spider. The resonance of 88 Hz is observed from the frequency response and is shown with dashed line in Fig. 5.5. The frequency response and the resonance are offset by the supply frequency of 50 Hz as was in the simulations. It can be seen that the shape of the current PSD is similar to the simulated case. However, the damping seems to be high enough that the resonance can't be observed from the current in this case even thought the excitation amplitude is selected according to typical guidelines for similar mechanical systems.

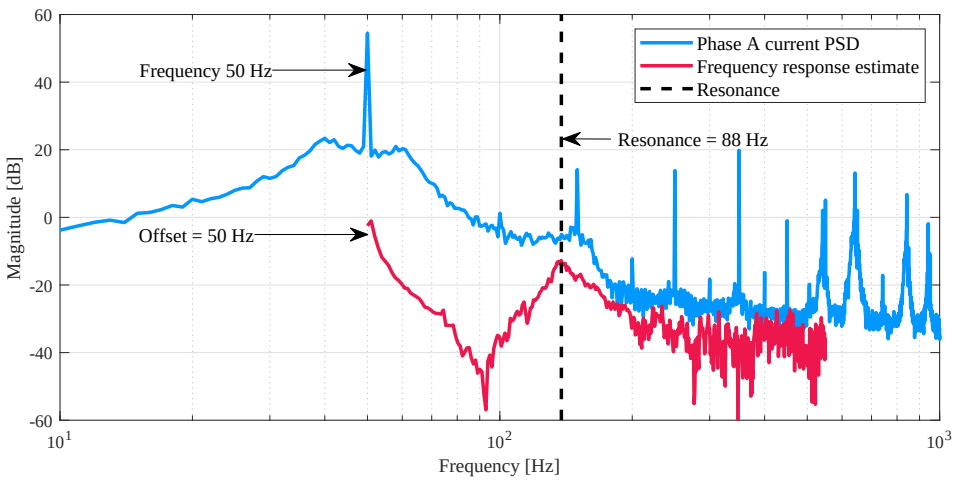

Figure 5.5: The Welch PSD of the phase A current signal from the DOL mechanical ID-experiment and the frequency response estimate obtained with the setup presented in Chapter 4.

6 Conclusions and summary

Vibration analysis is an important phase of a mechanical design. The main outcome of the vibration analysis is to secure safe operation on the operation range of the motor. However, smaller machines, and also larger machines to some extent, continue to produce problems related to torsional vibrations since they are hard to detect without external measurement tools. Typically, the torsional analysis after the delivery requires expensive and time consuming measurements. During commissioning of a VFD application a ”mechanical identification” -feature could be beneficial to detect critical speeds that should be avoided.

In this thesis, the identifiability of the first torsional natural frequency from selected signals of a VFD system is studied. The research is carried out with simulations and laboratory experiments. The mechanical system used in the simulations and experiments is simplified to a two-mass system representing a motor and a load that are connected with a coupling. The studied signals were torque, rotational speed and stator current of the motor from which the first two are obtained from the VFD and the latter is measured with an external power analyzer in the experiments. A PRBS signal is used as an excitation signal in all the experiments and simulations. The signals are analyzed in frequency domain using Welch’s power spectrum density estimate. The frequency responses from the system are estimated with Welch method. The experiment was first carried out as a closed-loop system. In addition, the stator current was also studied in DOL application where the motor is supplied directly from the 400 V, 50 Hz grid. The experiment is repeated for three different loads and for two different couplings.

As the used couplings allow backlash the torsional stiffness becomes undefined as the applied torque approaches zero. The effects of the backlash and the non-linearity of the coupling are emphasized with smaller loads due to the ratio of the PRBS amplitude and the static load torque which causes the motor torque to be transitively negative. The system’s mechanical frequency response was first estimated with the Welch method from the closed-loop system using the speed feedback from the encoder. The

resonance frequency obtained from the frequency response is used as a reference for the other identification methods. The experiments show positive results for sensorless identification of the resonance. From the studied signals, the resonance frequency was clearly visible in the PSD of the VFD's estimated rotational speed. From the frequency response from the excitation signal to the torque, the resonance was also observable to some extent. The resonance could not be identified from the stator current in the closed-loop case. The simulations of the DOL case show that with higher torsional damping the resonance becomes harder to observe from the current signal. The DOL experiments show similar results to the simulations. However, the damping of the coupling seems to be high enough that the resonance was not clearly visible.

As conclusion, the proposed method to identify the torsional natural frequency from the speed estimate could be developed more towards the integrated feature of a VFD. As the test lasts for 10 seconds, the method provides a solution for a fast estimation of the mechanical resonance. The applicability for condition monitoring should be investigated more since a constant excitation would most likely disturb the actual process' performance.

References

ABB (2019). *Firmware manual - ACS880 primary control program*. ABB industrial drives. Version: 3AUA0000085967.

API 684 (2005). *API Standard Paragraphs Rotordynamic Tutorial: Lateral Critical Speeds, Unbalance Response, Stability, Train Torsionals, and Rotor Balancing*, 2nd edn. Standard. Washington, D.C., USA: American Petroleum Institute.

Corbo, M.A. and Malanoski, S.B. (1996). Practical Design against Torsional Vibrations. In: *25th Turbomachinery Symposium Proceedings*, pp. 189–222.

Corriou, J.P. (2004). *Process control: Theory and Applications*. London, United Kingdom: Springer-Verlag. ISBN 1-85233-776-1.

Dimarogonas, A.D., Paipetis, S.A., and Chondros, T.G. (2013). *Analytical Methods in Rotor Dynamics*, 2nd edn. Dordrecht, Netherlands: Springer. ISBN 978-94-007-5905-3.

Friswell, M.I., Penny, J.E.T., Garvey, S.D., and Lees, A.W. (2010). *Dynamics of Rotating Machines*. New York, NY, USA: Cambridge University Press. ISBN 978-0-521-85016-2.

Holopainen, T., Niiranen, J., Jörg, P., and Andreo, D. (2013). Electric Motors and Drives in Torsional Vibration Analysis and Design. In: *Proceedings of the 42nd Turbomachinery Symposium*. Houston, TX, USA.

Hynynen, K. (2011). *Broadband Excitation in the System Identification of Active Magnetic Bearing Rotor Systems*. Ph.D. thesis. Lappeenranta University of Technology, Lappeenranta, Finland.

Isermann, R. (1981). *System Identification: Tutorials Presented at the 5th IFAC Symposium on Identification and System Parameter Estimation, F.R. Germany, September 1979*. Oxford, England: Published for the International Federation of Automatic Control by Pergamon Press. ISBN 0-08-027583-4.

Isermann, R. and Münchhof, M. (2011). *Identification of Dynamic Systems*. Berlin Heidelberg, Germany: Springer-Verlag. ISBN 978-3-540-78878-2.

Kaukonen, J. (1999). *Salient Pole Synchronous Machine Modelling in an Industrial Direct Torque Controlled Drive Application*. Ph.D. thesis. Lappeenranta University of Technology, Lappeenranta, Finland.

KTR (2020). *Drive Technology - Couplings, Torque Limiters, Clamping Elements, Torque Measuring Systems*. KTR catalog, pp. 32–33.

Ljung, L. (1987). *System Identification - Theory for the User*. Englewood Cliffs, NJ, USA: Prentice Hall, Inc. ISBN 0-13-881640-9.

Mauri, M., Rossi, M., and Bruha, M. (2016). Generation of Torsional Excitation in a Variable-Speed-Drive System. In: *International Symposium on Power Electronics, Electrical Drives, Automation and Motion*, pp. 516–521. Anacapri, Italy.

Mohammed, N., Ciobotaru, M., and Town, G. (2019). Performance Evaluation of Wideband Binary Identification of Grid Impedance Using Grid-connected Inverters. In: *21st European Conference on Power Electronics and Applications*, pp. 1–10. Genova, Italy. doi: 10.23919/EPE.2019.8915509.

Nevaranta, N. (2016). *Online Time and Frequency Domain Identification of a Resonating Mechanical System in Electric Drives*. Ph.D. thesis. Lappeenranta University of Technology, Lappeenranta, Finland.

Niiranen, J. (2000). *Sähkömoottorikäytön digitaalinen ohjaus*. Helsinki, Finland: Otatieto Oy Yliopistokustannus University Press Finland. ISBN 951-672-300-4.

Orkisz, M. and Ottewill, J. (2012). Detecting Mechanical Problems by Examining Variable Speed Drive Signals. In: *International Symposium on Power Electronics, Electrical Drives, Automation and Motion*, pp. 1366–1371. Sorrento, Italy. doi:10.1109/SPEEDAM.2012.6264466.

Pintelon, R. and Schoukens, J. (2001). *System Identification: A Frequency Domain Approach*. New York, NY, USA: IEEE Press. ISBN 0-7803-6000-1.

Saarakkala, S. and Hinkkanen, M. (2015). Identification of Two-Mass Mechanical Systems Using Torque Excitation: Design and Experimental Evaluation. *IEEE Transactions on Industry Applications*, 51(5), pp. 4180–4189. doi:10.1109/TIA.2015.2416128.

Schoukens, J., Pintelon, R., van der Ouderaa, E., and Renneboog, J. (1988). Survey of Excitation Signals for FFT Based Signal Analyzers. *IEEE Transactions on Instrumentation and Measurement*, 37(3), pp. 342–352. doi:10.1109/19.7453.

Schramm, S., Sihler, C., Song-Manguelle, J., and Rotondo, P. (2010). Damping Torsional Interharmonic Effects of Large Drives. *IEEE Transactions on Power Electronics*, 25(4), pp. 1090–1098. doi: 10.1109/TPEL.2009.2033274.

Stoica, P. and Moses, R. (2005). *Spectral analysis of signals*. Upper Saddle River, NY, USA: Prentice Hall, Inc. ISBN 0-13-113956-8.

Vilkko, M. and Roinila, T. (2008). Designing Maximum Length Sequence Signal for Frequency Response Measurement of Switched Mode Converters. In: *NORPIE/2008, Nordic Workshop on Power and Industrial Electronics*. Espoo, Finland.

Villwock, S. and Pacas, M. (2008). Application of the Welch-method for the Identification of Two- and Three-Mass-Systems. *IEEE Transactions on Industrial Electronics*, 55(1), pp. 457–466. doi: 10.1109/TIE.2007.909753.

Vulfson, I. (2015). *Dynamics of Cyclic Machines*. Cham, Germany: Springer International Publishing. ISBN 978-3-319-12634-0.

Vuojolainen, J., Nevaranta, N., Jastrzebski, R., and Pyrhönen, O. (2017). Comparison of Excitation Signals in Active Magnetic Bearing System Identification. *Modeling, Identification and Control*, 38(1), pp. 1–11. doi:10.4173/mic.2017.1.1.

Wahrburg, A., Jelavic, E., Klose, S., and Listmann, K. (2017). Robust Semi-Automatic Identification of compliantly Coupled Two-Mass Systems. *International Federation of Automatic Control*, 50(1), pp. 14569–14574. doi:10.1016/j.ifacol.2017.08.2097.

Weber, A.R., Weissbacher, J., Steiner, G., and Horn, M. (2014). An Accurate Auto-Tuning Procedure for Encoderless AC Motor Drives in Industrial Environments. *Transactions on Electrical Engineering*, 3(1), pp. 1–7.

Welch, P.D. (1967). The Use of Fast Fourier Transform for the Estimation of Power Spectra: A Method Based on Time Averaging Over Short, Modified Periodograms. *IEEE Transactions on Audio and Electroacoustics*, AU-15(2), pp. 70–73. doi:10.1109/TAU.1967.1161901.

Zoubek, H. and Pacas, M. (2011). Two Steps towards Speed Estimation and Encoderless Identification of Two-Mass-Systems with Extended Speed Adaptive Observer Structure. In: *IECON 2011 - 37th Annual Conference of the IEEE Industrial Electronics Society*, pp. 2072–2077. Melbourne, Australia. doi:10.1109/IECON.2011.6119627.

Zoubek, H. and Pacas, M. (2017). Encoderless Identification of Two-Mass-Systems Utilizing an Extended Speed Adaptive Observer Structure. *IEEE Transactions on Industrial Electronics*, 64(1), pp. 595–604. doi:10.1109/TIE.2016.2598521.